THE JOURNAL OF PHYSICAL CHEMISTRY B

Article

pubs.acs.org/JPCB

Growth Kinetics of Nanoclusters in Solution

Awaneesh Singh,[†,‡] Sanjay Puri,*[,†] and Chandan Dasgupta[‡]

[†]School of Physical Sciences, Jawaharlal Nehru University, New Delhi - 110067, India

[‡]Department of Physics, Indian Institute of Science, Bangalore - 560012, India

ABSTRACT: We study the growth kinetics of nanoclusters in solution. There are two generic factors that drive growth: (a) reactions that produce the nanomaterial; and (b) diffusion of the nanomaterial due to chemical-potential gradients. We model the growth kinetics of ZnO nanoparticles via coupled dynamical equations for the relevant order parameters. We study this model both analytically and numerically. We find that there is a crossover in the nanocluster growth law: from $L(t) \sim t^{1/2}$ in the *reaction-controlled* regime to $L(t) \sim t^{1/3}$ in the *diffusion-controlled* regime.

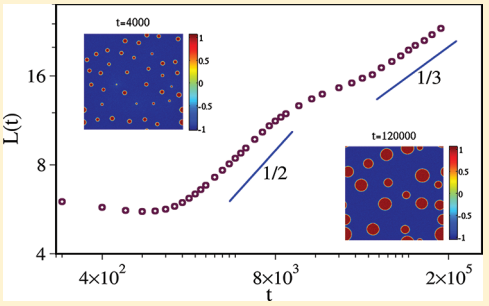

INTRODUCTION

There has been great research interest in the growth of a minority phase in a background of the majority phase.[1−5] A well-established scenario for this growth process is *Ostwald ripening*, where larger droplets or clusters grow at the expense of smaller clusters. The pioneering work on Ostwald ripening is due to Lifshitz and Slyozov[1] and (independently) Wagner.[2] These authors obtained an elegant asymptotic solution for the evolution of an ensemble of droplets in the limit of vanishing minority phase. They also found that Ostwald ripening is characterized by the growth of a unique time-dependent length scale, $L(t) \sim t^{1/3}$. This result is referred to as the Lifshitz−Slyozov−Wagner (LSW) growth law and has been confirmed in many experiments[6,7] and simulations.[8]

In recent years, there has also been considerable interest in the growth kinetics of quantum nanomaterials.[9,10] In particular, attention has focused on the applicability of Ostwald ripening to the growth of metal-oxide nanoclusters from solution. An understanding of the growth process would provide control in technological applications concerning the optical, electrical, and magnetic properties of a nanomaterial.[11−13] There are many experimental results that confirm LSW kinetics for the late stages of nanocluster growth in TiO_2,[14] InAs and CdSe,[15] and ZnO.[16]

However, several recent experimental studies have shown that LSW theory is inadequate for a complete description of nanocluster growth.[17−19] These have also been supplemented by theoretical investigations.[19−21] For example, Viswanatha et al.[18] have studied the growth of ZnO nanoclusters in solution. They have shown that the growth process is qualitatively different from Ostwald ripening, and shows a crossover from *reaction-limited* growth at early times (with $L(t) \sim t^{1/2}$ [22,23]) to *diffusion-limited* LSW growth at late times. Clearly, this is a generic scenario that is applicable to a wide range of experiments on nanoparticle and crystal growth. Therefore, we would like to have a theoretical understanding of this scenario. In this paper, we undertake an analytical and numerical study of pattern formation in the growth of nanoclusters. We formulate and study a phenomenological model for this problem. Our study is motivated by the experiments of Viswanatha et al. on ZnO growth.[18] However, the theoretical framework we develop is applicable in a much wider experimental context.

MODELING OF ZNO NANOCLUSTER GROWTH

Experimental Details. In the experiments of Viswanatha et al.,[18] ZnO nanoclusters were synthesized using water (H_2O) and zinc acetate [$Zn(CH_3COO)_2$] The specific choice of this reaction was due to the observation that the presence of a small amount of water in the synthesis of ZnO nanoclusters strongly influences the size of the nanoclusters.[24] The growth process was initiated by adding 0.1 mmol of zinc acetate to 100 mL of 100−250 mM solution of double-distilled water in isopropenol (i-PrOH). The solution was maintained in a water bath at the required temperature (301−338 K). The growth of ZnO nanoclusters in real time was monitored by in situ time-resolved optical-absorption spectra. The well-known shifts of the band gaps, and consequently of the absorption edges with size, provided a reliable way to extract the average size and size distribution of the growing nanocluster assembly.[13,25]

The growth of a ZnO nanocluster via the solution route is controlled by two processes. First, there is a reaction at the surface of the cluster producing ZnO, which is incorporated into the cluster. Second, there is diffusion of Zn ions to the surface of the growing cluster. Let us focus on the reaction, which involves the dissociation of zinc acetate, providing Zn^{2+} ions. Furthermore, hydroxyl ions (OH^-) are produced in the solution from the dissociation of water. The nanoclusters of ZnO are comprised of tetrahedrally coordinated Zn and O atoms, and only the surface Zn atoms are terminated with an OH^- ion instead of an O atom. The reaction-driven growth of a nanocluster proceeds by the dehydration of terminating OH^- ions using the

Received: November 26, 2011
Revised: March 16, 2012
Published: March 16, 2012

   dx.doi.org/10.1021/jp211380j | *J. Phys. Chem. B* 2012, 116, 4519−4523

freely available OH^- ions in the solution. This is followed by the capture of free Zn^{2+} ions near the surface of the nanoclusters.

The Zn^{2+} ions and the OH^- ions in the solution can be considered as monomers of the growth process. The growth of the nanocluster proceeds with a Zn^{2+} ion capturing an OH^- ion and so on. Thus, the reaction, namely, $H_2O \rightleftharpoons H^+ + OH^-$, $Zn^{2+} \rightleftharpoons 2OH^- \rightleftharpoons Zn(OH)_2 \rightleftharpoons ZnO + H_2O$, is controlled by (a) the diffusion of Zn^{2+} ions, and (b) the rate at which reactions take place at the surface. Both of these mechanisms have to be taken into account in modeling the reaction-driven growth process. During the reaction, the local concentration of ZnO increases with time, while the concentration of Zn^{2+} decreases. Since the total number of Zn atoms (either in ZnO or in the form of Zn^{2+} ions) is conserved, the increase of ZnO must be compensated by the decrease of Zn^{2+} ions.

Phenomenological Modeling. We denote the local concentration of ZnO as $c(\vec{r}, t)$. The values of c range from 0 (no ZnO and all solvent) to 1 (all ZnO and no solvent). The corresponding order parameter is $\psi(\vec{r}, t) = 2c(\vec{r}, t) - 1$; $\psi \simeq +1$ and $\psi \simeq -1$ denote regions that are ZnO-rich and ZnO-poor, respectively. In the absence of any reaction, ψ obeys the Cahn–Hilliard–Cook (CHC) equation:[26,27]

$$\frac{\partial}{\partial t}\psi(\vec{r}, t) = \vec{\nabla}\cdot\{\vec{\nabla}(-\psi + \psi^3 - \nabla^2\psi) + \vec{\theta}(\vec{r}, t)\} \quad (1)$$

Here, we have used the dimensionless version of the CHC equation, which is obtained by a suitable rescaling of space, time, and order parameter.[5] The Gaussian white noise term $\vec{\theta}(\vec{r}, t)$ has zero average and obeys the following fluctuation–dissipation relation:

$$\langle\theta_i(\vec{r}', t')\theta_j(\vec{r}'', t'')\rangle = 2\varepsilon\delta_{ij}\delta(\vec{r}' - \vec{r}'')\delta(t' - t'') \quad (2)$$

where ε is the noise strength (proportional to the system temperature). The CHC equation models diffusion-limited coarsening in which growing ZnO nanoclusters would obey the LSW growth law, $L(t) \sim t^{1/3}$.[8]

Next, we incorporate the chemical reaction that converts Zn^{2+} to ZnO and vice versa. We make the following assumptions about the reaction (motivated by the experimental observations): (1) The reaction occurs at the surface of the ZnO clusters. (2) The rate of conversion of Zn^{2+} to ZnO (k_f) is much faster than that of the reverse reaction (k_b), i.e., $k_f \gg k_b$. The local time-dependent concentration of Zn^{2+} is denoted by the dimensionless quantity $c_1(\vec{r}, t)$ with $0 \le c_1 \le 1$. The rate equation obeyed by $c_1(\vec{r}, t)$ is

$$\frac{\partial}{\partial t}c_1(\vec{r}, t) = f(\psi)(-k_f[OH^-]^2c_1 + k_b[H_2O]c) + D\nabla^2c_1 \quad (3)$$

where $[OH^-]$ and $[H_2O]$ denote the concentrations of hydroxyl ion and water, respectively. (We assume that these concentrations remain constant throughout the process. Therefore, they can be absorbed into the rate constants.) In eq 3, the factor $f(\psi)$ localizes the reaction to the surface of the nanoclusters where $\psi \simeq 0$. We have considered several different functional forms of $f(\psi)$, all of which yield similar results. The results presented in this paper correspond to $f(\psi) = \exp(-\gamma\psi^2)$.

We introduce the order parameter for Zn^{2+} ions as $\phi(\vec{r}, t) = 2c_1(\vec{r}, t) - 1$. Then, eq 3 can be rewritten as

$$\frac{\partial}{\partial t}\phi(\vec{r}, t) = -\lambda e^{-\gamma\psi^2}[(1 + \phi) - \alpha(1 + \psi)] + D\nabla^2\phi \quad (4)$$

where $\lambda = k_f[OH^-]^2$ and $\alpha = k_b[H_2O]/(k_f[OH^-]^2)$. As the total number of Zn atoms is conserved, the depletion of Zn^{2+} ions corresponds to an increase in the number of ZnO molecules. Therefore, in the presence of the chemical reaction, eq 1 is modified to

$$\frac{\partial}{\partial t}\psi(\vec{r}, t) = \vec{\nabla}\cdot[\vec{\nabla}(-\psi + \psi^3 - \nabla^2\psi) + \vec{\theta}(\vec{r}, t)] + \lambda e^{-\gamma\psi^2}[(1 + \phi) - \alpha(1 + \psi)] \quad (5)$$

The coupled eqs 4 and 5 describe the evolution dynamics of our experimental system. In earlier works, Puri and Frisch[28] and Glotzer et al.[29,30] have considered the phase separation of binary (AB) mixtures with simple chemical reactions, e.g., $A \rightleftharpoons B$, $AB \rightleftharpoons BB$, etc. The resultant phenomenological models are of the same form as eq 5, i.e., the CHC equation in conjunction with a nonconserving term due to the reaction. The novel feature of our present model is the dynamical interplay of segregation and reaction kinetics.

Let us examine the evolution of our model (with noise amplitude $\varepsilon = 0$) from a homogeneous initial condition with $\phi = \phi_0$ and $\psi = -1$, i.e., there are no ZnO nanoclusters at $t = 0$. The values of the spatial averages $\bar{\phi}$and $\bar{\psi}$ change slowly: $\bar{\phi}(t) = \phi_0 - h(t)$ and $\bar{\psi}(t) = -1 + h(t)$, where

$$\frac{dh}{dt} = \lambda e^{-\gamma(-1+h)^2}[1 + \phi_0 - (1 + \alpha)h], \quad h(0) = 0 \quad (6)$$

The short-time solution of eq 6 is $h(t) \simeq \lambda e^{-\gamma}(1 + \phi_0)t$ and the fixed point is $h^* = (1 + \phi_0)/(1 + \alpha)$. During this evolution, the ψ-field may develop composition inhomogeneities via *nucleation and growth* for $-1 \le \bar{\psi}(t) \le -1/\sqrt{3}$, or via *spinodal decomposition* for $-1/\sqrt{3} \le \bar{\psi}(t)$. Our primary interest in this paper is the nature of pattern dynamics in the inhomogeneous system, which we discuss in the next section. As discussed in the next section, the initial conditions for our simulations consist of a few ZnO seeds (with $\psi = 1$) distributed uniformly in a background of $\psi = -1$. Therefore, the growth process may be classified as nucleation and growth. Even at late times, $\bar{\psi}(t)$ stays below the threshold for spinodal decomposition.

DETAILED NUMERICAL RESULTS

We implemented an Euler-discretized version of eqs 4 and 5, with an isotropic Laplacian on a square lattice of size $L_x \times L_y = 512^2$. Periodic boundary conditions were imposed in both directions. The discretization mesh sizes in space and time were $\Delta x = 1.0$ and $\Delta t = 0.02$, respectively. We have confirmed that the spatial mesh size Δx is sufficiently small to resolve the interface region, where most of the reaction dynamics occurs. The initial condition for a run consisted of a few ZnO nanoclusters (with $\psi = 1$) distributed randomly in a background of $\psi = -1$. These initial seeds were of random sizes (5–7 in dimensionless units) and well-separated from each other.

In our simulation, the initial order-parameter value for Zn^{2+} ions was $\phi_0 = -0.6$. The thermal noise of strength ε is modeled by uniformly distributed random numbers between $[-A,A]$ with $A = [3\varepsilon/(\Delta x)^d\Delta t]^{1/2}$ [31] (the spatial dimension d is equal to 2 in our calculation). We set $A = 1$, corresponding to $\varepsilon = 6.7 \times 10^{-3}$ in eq 5. The results reported here correspond to the parameter values $\gamma = 40$, $\alpha = 0.1$, $D = 1.0$, and $\lambda = 0$ (no reaction), 0.01, 0.02, and 0.04.

In Figure 1, we show the evolution of ZnO nanoclusters for the case with $\lambda = 0.02$. The evolution snapshots correspond to

dx.doi.org/10.1021/jp211380j | J. Phys. Chem. B 2012, 116, 4519–4523

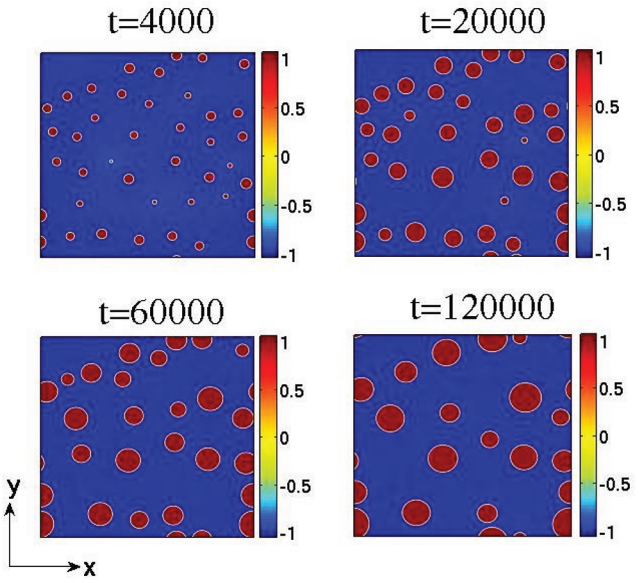

Figure 1. Evolution of ZnO nanoclusters obtained from a numerical solution of our model in eqs 4 and 5. The parameter values are λ = 0.02, γ = 40, α = 0.1, and D = 1.0. The discretization mesh sizes are Δx = 1.0 and Δt = 0.02. The system size is 512^2 and periodic boundary conditions are applied in both directions. The noise amplitude is ε = 0.0067. The initial condition consisted of a few ZnO nanoclusters (ψ = 1) of random sizes (and at random positions) in a background of ψ = −1. The color-bars on the right of each frame clearly differentiate the growth of ZnO clusters (red droplets) in a background of $\psi \simeq -1$.

the dimensionless times mentioned. At t = 4000, the clusters are well-separated from each other. At early times, Zn^{2+} converts to ZnO, which deposits on the growing droplets. At later times, when Zn^{2+} ions have been depleted, the clusters grow via Ostwald ripening, with larger droplets growing at the expense of smaller droplets. In Figure 2, we show the order

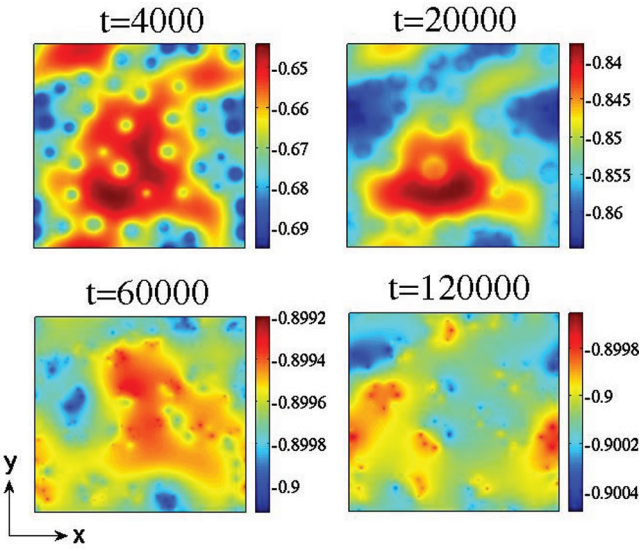

Figure 2. Concentration variation of Zn^{2+} ions for the system shown in Figure 1. The Zn^{2+} ion concentration is minimum near the cluster surface due to the conversion of Zn^{2+} into ZnO.

parameter of Zn^{2+} ions for the evolution depicted in Figure 1. As the chemical reaction that converts Zn^{2+}ions into ZnO occurs at the surface of the clusters, the Zn^{2+} concentration is minimum near the cluster surface. It gradually increases as we move away from the cluster surface. Notice that the average value of the ϕ-field diminishes with time, as seen from the color-bar scales.

Figure 3 shows the variation of the ZnO order parameter (ψ) in the snapshots of Figure 1, along a horizontal cross-section at

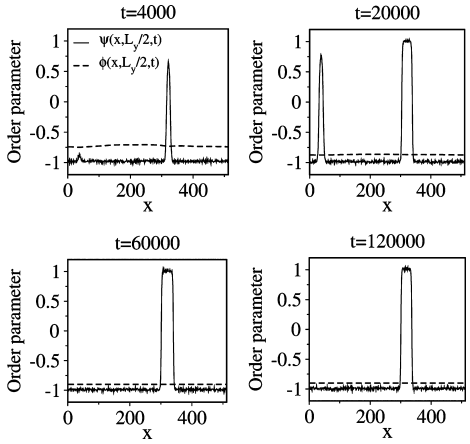

Figure 3. Order-parameter profiles for the evolution snapshots of Figures 1 and 2. We show the variation of ψ and ϕ along a horizontal cross-section at the center of the vertical axis: $y = L_y/2$.

the center of the vertical y-axis. We also show the corresponding variation of ϕ (order parameter of Zn^{2+}). The depletion of ϕ at the droplet interfaces ($\psi \simeq 0$) is not apparent on this scale. In Figure 4, we show the time-dependence of the average values

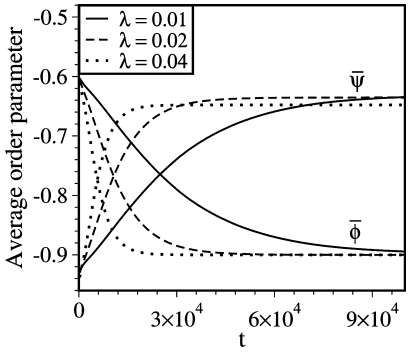

Figure 4. Time-dependence of the spatial averages of $\bar{\psi}(\vec{r}, t)$ and $\phi(\vec{r}, t)$ for λ = 0.01, 0.02, and 0.04.

$\bar{\psi}(t) = V^{-1}\int d\vec{r}\psi(\vec{r}, t)$ and $\bar{\phi}(t) = V^{-1}\int d\vec{r}\phi(\vec{r}, t)$, where V is the system volume. We show results for different values of λ in Figure 4.

The cluster morphology is studied experimentally using the order-parameter *correlation function*:[5]

$$C(\vec{r}, t) = \frac{1}{V}\int d\vec{R}[\langle\psi(\vec{R}, t)\psi(\vec{R} + \vec{r}, t)\rangle - \langle\psi(\vec{R}, t)\rangle\langle\psi(\vec{R} + \vec{r}, t)\rangle] \quad (7)$$

In eq 7, the angular brackets denote an averaging over independent runs. All statistical quantities presented in this paper are obtained on 512^2 systems as averages over 10 runs. As the system is translationally invariant and isotropic, $C(\vec{r}, t)$

dx.doi.org/10.1021/jp211380j | J. Phys. Chem. B 2012, 116, 4519–4523

depends only on $|\vec{r}| = r$. The existence of a characteristic domain scale $L(t)$ results in the *dynamical scaling* of $C(\vec{r}, t)$:

$$C(\vec{r}, t) = C(r, t) = g(r/L) \tag{8}$$

where $g(x)$ is a scaling function.

Let us study the correlation function for the evolution shown in Figure 1. In Figure 5, we plot $C(r,t)$ versus r/L at the same times as in Figure 1. The length scale $L(t)$ is obtained as the distance over which the correlation function decays to half its maximum value $[C(r = 0, t)]$. In the early stages of the dynamics, the system is chemically active and Zn^{2+} ions are converted to ZnO. There is an ongoing depletion of Zn^{2+} up to $t_c \simeq 5 \times 10^4$ (see Figure 4), and a corresponding increase in the average value $\bar{\psi}(t)$. Thus, the composition (*off-criticality*) of the segregating ZnO-field changes while the system is chemically active. As the correlation function depends on the off-criticality $\bar{\psi}(t)$,[8] there is a crossover in the scaled correlation function shown in Figure 5. This is manifested as a scaling breakdown near the minimum of $C(r, t)$ $(r/L > 2)$. The function $C(r, t)$ only settles to its asymptotic scaling form for $t > t_c \simeq 5 \times 10^4$, and obeys dynamical scaling once the system is in this chemically inactive regime. In the asymptotic regime, cluster growth proceeds via an *evaporation−condensation mechanism*. ZnO *evaporates* from smaller droplets with higher chemical potential and is diffusively transported through the solvent-rich regions. This ZnO *condenses* on larger droplets that have lower chemical potential, thereby driving their growth. This is the usual Ostwald ripening process.

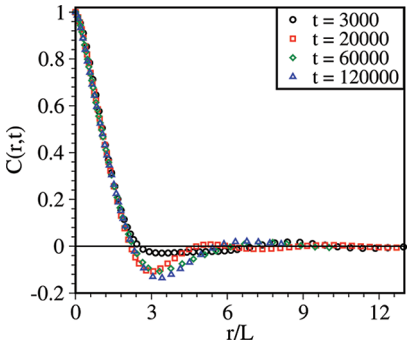

Figure 5. Scaling plot of correlation function $[C(r, t)$ vs $r/L]$ at different times. In the chemically active system, the data sets do not show dynamical scaling as the average value of the order parameter $\bar{\psi}(t)$ changes with time. However, at late times, when the system becomes chemically inactive, the data sets collapse onto a scaling curve. This statistical data is obtained on a 512^2 system as an average over 10 independent runs.

In Figure 6a, we plot the time-dependence of the domain size $[L(t)$ vs $t]$ for nanocluster growth with different values of λ. First, we observe that, without the chemical reaction $(\lambda = 0)$, the system follows the usual LSW growth law, $L(t) \sim t^{1/3}$. Next, we discuss the role of the chemical reaction. In the early stages, the system is chemically active, and the nanoclusters exhibit a *reactive growth* regime. A quantitative understanding of the reactive and diffusive regimes can be obtained from the growth equation due to Sugimoto[22] for a droplet of size r:

$$\frac{dr}{dt} = \frac{\alpha}{r^2}\left(\frac{r/r_c - 1}{D^{-1} + (kr)^{-1}}\right) \tag{9}$$

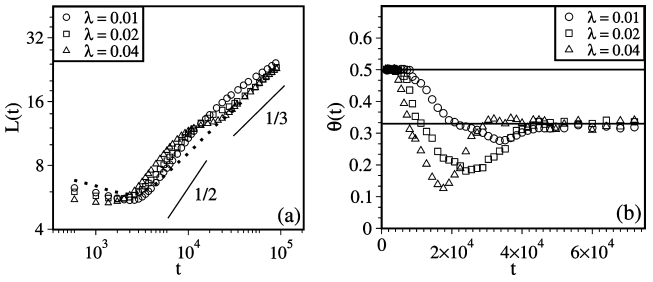

Figure 6. (a) Time-dependence of domain size, $L(t)$ vs t, for the evolution depicted in Figure 1. The length scale $L(t)$ is defined as the distance over which $C(r,t)$ decays to half its maximum value (at $r = 0$). We show length-scale data for $\lambda = 0.01, 0.02, 0.04$. For comparison, we also show results (dotted line) for the usual CHC model ($\lambda = 0$, no reaction). The solid lines denote the growth laws $L(t) \sim t^{1/2}$ and $L(t) \sim t^{1/3}$. (b) Variation of the instantaneous growth exponent θ with time.

Here, α is a material parameter, D is the diffusion constant for Zn^{2+} ions in the solvent, and k measures the reaction rate. In eq 9, $r_c(t)$ is the time-dependent critical cluster size that depends upon the supersaturation. At a given time, droplets with $r > r_c$ grow, whereas those with $r < r_c$ shrink. Following ref 18, we replace r by the average cluster size l and assume that the factor l/r_c on the right-hand side (RHS) of eq 9 is constant in time. The reactive regime corresponds to $kl \ll D$ with $l(t) \sim (\alpha k t)^{1/2}$. After a crossover time $t_c \sim D^2/(\alpha k^3)$, the subsequent growth of the droplets occurs via Ostwald ripening with $l(t) \sim (\alpha D t)^{1/3}$. These two regimes are clearly seen in Figure 6a. In Figure 6b, we plot the *instantaneous exponent* θ $[= d(\ln L)/d(\ln t)]$ versus t. This figure clearly exhibits the two limiting values of the growth exponent: $\theta = 1/2$ in the early time reactive regime, and $\theta = 1/3$ in the late-time diffusive regime. As expected, the crossover to the asymptotic regime is faster for higher values of λ, corresponding to a faster reaction rate. The transition from the reactive regime to the Ostwald ripening regime can be observed in various morphological properties. In Figure 5, we have demonstrated that there is a crossover in the scaling form of the correlation function. We also observe a corresponding change in the droplet size distribution.[19] For the sake of brevity, we do not show these results here.

We have also studied the growth of single droplets of ZnO $(\psi = 1)$ in a background of pure solvent $(\psi = -1)$. In this case, there is no possibility of Ostwald ripening or LSW growth. In the presence of the reaction, the droplet grows as $L(t) \sim t^{1/2}$. However, when the Zn^{2+} ions are fully depleted, there is no further growth of the single droplet.

Before concluding this section, it is useful to discuss some related studies of crossovers in coarsening dynamics. For example, Schmelzer et al.[32] have observed a similar transition $(t^{1/2} \rightarrow t^{1/3})$ in their numerical studies of the growth of AgCl nanoclusters. They attribute the initial $t^{1/2}$ behavior to "independent" growth which, we believe, is similar to the reaction-controlled growth found in our study: as noted above, the size of a single droplet of ZnO in a background of pure solvent grows as $t^{1/2}$ in our model. Another mechanism that may lead to early time growth behavior that is different from Ostwald ripening is the *coalescence* of clusters. A crossover from an early time regime of coalescence-induced growth to an asymptotic Ostwald ripening regime has been observed in a Monte Carlo simulation[33] of coarsening in thin films. Pawluk and Wong[34] have used *ab initio* molecular dynamics simulations to show that the process of coalescence leads to the formation of low-energy iridium clusters, and the experimental studies of Tiemann et al.[35]

dx.doi.org/10.1021/jp211380j | J. Phys. Chem. B 2012, 116, 4519−4523

have emphasized the importance of coalescence processes in the growth of ZnS nanoparticles. Coalescence-induced growth may be distinguished from the reaction-controlled growth found in our study by either the value of the growth exponent[33] or the shape of the droplet size distribution.[36]

SUMMARY AND DISCUSSION

Let us conclude this paper with a summary and discussion of our modeling and results, which have been motivated by experiments on nanocluster growth. In particular, we have focused on the growth of ZnO nanoparticles from a solution of zinc acetate and water.[18] The growth of nanoclusters has two generic components: (a) There is a reaction at the cluster surface, and the reaction product is incorporated into the droplet. (b) There is *diffusion* of the nanomaterial to the surface of the droplet. Our goal in this paper has been the formulation of a phenomenological model for this process. This would constitute the starting point of analytical and numerical studies of this technologically important problem.

Starting from the equations for the chemical reaction, we have formulated a coupled dynamical model for the evolution of two order parameters: $\psi(\vec{r}, t)$, which measures the concentration of ZnO nanomaterial; and $\phi(\vec{r}, t)$, which measures the concentration of Zn^{2+} ions. The evolution of $\psi(\vec{r}, t)$ is governed by the usual CHC equation for phase separation in conjunction with a chemical-reaction term, which is confined to the surface of ZnO nanoclusters. On the other hand, the kinetics of $\phi(\vec{r}, t)$ is dictated by the ongoing chemical reaction. We have presented results from an analytical and numerical study of this model. The following significant results emerge from our study. First, there is a crossover in the nanocluster growth law: from $L(t) \sim t^{1/2}$ in the reaction-controlled regime to $L(t) \sim t^{1/3}$ in the diffusion-controlled Ostwald ripening regime. Second, there is a crossover in the scaling form of the correlation function of the ZnO concentration field. This is due to the continuous change in the off-criticality $\bar{\psi}(t)$ of the solution as the reaction proceeds. The correlation function settles to an asymptotic scaling form at long times, when $\bar{\psi}(t)$ reaches a constant value after the reactants have been depleted.

Given the current focus on nanomaterials and their properties, we hope that this paper will motivate fresh interest in the evolution dynamics and morphology of nanoclusters. These kinetic processes play an important role in determining the functionality of nanomaterials. We emphasize that one can gain a good understanding of the relevant pattern dynamics from simple coarse-grained models of the type discussed here.

AUTHOR INFORMATION

Notes

The authors declare no competing financial interest.

ACKNOWLEDGMENTS

AS and CD thank the Department of Science and Technology (DST), Government of India, and MONAMI (Indo-EU project) for financial support. We are also grateful to D.D. Sarma and R. Viswanatha for many useful discussions.

REFERENCES

(1) Lifshitz, I. M.; Slyozov, V. V. *J. Phys. Chem. Solids* **1961**, *19*, 35−50.
(2) Wagner, C. Z. *Elektrochem.* **1961**, *65*, 581−591.
(3) Bray, A. J. *Adv. Phys.* **1994**, *43*, 357−459.
(4) Binder, K.; Fratzl, P. In *Phase Transformations in Materials*; Kostorz, G., Ed.; Wiley-VCH: New York, 2001; pp 409−480.
(5) Puri, S. *Kinetics of Phase Transitions*; Puri, S., Wadhawan, V. K., Eds.; CRC Press, Boca Raton, FL, 2009; pp 1−61.
(6) Carlow, G. R.; Zinke-Allmang, M. *Phys. Rev. Lett.* **1997**, *78*, 4601−4604.
(7) Alkemper, J.; Snyder, V. A.; Akaiwa, N.; Voorhees, P. W. *Phys. Rev. Lett.* **1999**, *82*, 2725−2728.
(8) Oono, Y.; Puri, S. *Phys. Rev. Lett.* **1987**, *58*, 836−839; *Phys. Rev. A* **1988**, *38*, 434−453. Puri, S.; Oono, Y. *Phys. Rev. A* **1988**, *38*, 1542−1565.
(9) Biswas, K.; Das, B.; Rao, C. N. R. *J. Phys. Chem. C* **2008**, *112*, 2404−2411.
(10) Caetano, B. L.; Santilli, C. V.; Meneau, F.; Briois, V.; Pulcinelli, S. H. *J. Phys. Chem. C* **2011**, *115*, 4404−4412.
(11) Patzke, G. R.; Zhou, Y.; Kontic, R.; Conrad, F. *Angew. Chem., Int. Ed.* **2011**, *50*, 826−859.
(12) Sapra, S.; Shanthi, N.; Sarma, D. D. *Phys. Rev. B* **2002**, *66*, 205202−205209.
(13) Sapra, S.; Sarma, D. D. *Phys. Rev. B* **2004**, *69*, 125304−125310.
(14) Oskam, G.; Nellore, A.; Penn, R. L.; Searson, P. C. *J. Phys. Chem. B* **2003**, *107*, 1734−1738.
(15) Peng, X.; Wickham, J.; Alivisatos, A. P. *J. Am. Chem. Soc.* **1998**, *120*, 5343−5344.
(16) Hu, Z.; Escamilla Ramirez, D. J.; Heredia Cervera, B. E.; Oskam, G.; Searson, P. C. *J. Phys. Chem. B* **2005**, *109*, 11209−11214.
(17) Seshadri, R.; Subbanna, G. N.; Vijaykrishnan, V.; Kulkarni, G. U.; Ananthakrishna, G.; Rao, C. N. R. *J. Phys. Chem.* **1995**, *99*, 5639−5644.
(18) Viswanatha, R.; Santra, P. K.; Dasgupta, C.; Sarma, D. D. *Phys. Rev. Lett.* **2007**, *98*, 255501−255504.
(19) Talapin, D. V.; Rogach, A. L.; Haase, M.; Weller, H. *J. Phys. Chem. B* **2001**, *105*, 12278−12285. Talapin, D. V.; Rogach, A. L.; Shevchenko, E. V.; Kornowski, A.; Haase, M.; Weller, H. *J. Am. Chem. Soc.* **2002**, *124*, 5782−5790.
(20) van Embden, J.; Sader, J. E.; Davidson, M.; Mulvaney, P. *J. Phys. Chem. C* **2009**, *113*, 16342−16355.
(21) Rempel, J. Y.; Bawendi, M. G.; Jensen, K. F. *J. Am. Chem. Soc.* **2009**, *131*, 4479−4489.
(22) Sugimoto, T. *Adv. in Coll. and Interf. Sci.* **1987**, *28*, 65−108.
(23) Du, D.; Srolovitz, D. J.; Coltrin, M. E.; Mitchell, C. C. *Phys. Rev. Lett.* **2005**, *95*, 155503−155506.
(24) Meulenkamp, E. A. *J. Phys. Chem. B* **1998**, *102*, 5566−5572.
(25) Viswanatha, R.; Sarma, D. D. *Chem.—Eur. J.* **2005**, *12*, 180−186.
(26) Cahn, J. W.; Hilliard, J. E. *J. Chem. Phys.* **1958**, *28*, 258−267.
(27) Cook, H. E. *Acta Metall.* **1970**, *18*, 297−306.
(28) Puri, S.; Frisch, H. L. *J. Phys. A: Math. Gen.* **1994**, *27*, 6027−6038; *Int. J. Mod. Phys. B* **1998**, *12*, 1623−1641.
(29) Glotzer, S. C.; Stauffer, D.; Jan, N. *Phys. Rev. Lett.* **1994**, *72*, 4109−4112.
(30) Glotzer, S. C.; Di Marzio, E. A.; Muthukumar, M. *Phys. Rev. Lett.* **1995**, *74*, 2034−2037.
(31) Puri, S.; Binder, K. *Phys. Rev. Lett.* **2001**, *86*, 1797−1800; *Phys. Rev. E* **2002**, *66*, 061602−061611.
(32) Schmelzer, J.; Lembke, U.; Kranold, R. *J. Chem. Phys.* **2000**, *113*, 1268−1275.
(33) Lo, A.; Skodje, R. T. *J. Chem. Phys.* **2000**, *112*, 1966−1974.
(34) Pawluk, T.; Wang, L. *J. Phys. Chem. C* **2007**, *111*, 6713−6719.
(35) Tiemann, M.; Marlow, F.; Hartikainen, J.; Weiss, O.; Linden, M. *J. Phys. Chem. C* **2008**, *112*, 1463−1467.
(36) Conti, M.; Meerson, B.; Peleg, A.; Sasorov, P. V. *Phys. Rev. E* **2002**, *65*, 046117−046129.

NOTE ADDED AFTER ASAP PUBLICATION

This paper was published on the Web on April 4, 2012. Changes have been made in equation 8 and in the text describing Figure 6b. The corrected version was reposted on April 10, 2012.